

INDUCTIVE ALIGNMENT FOR TABLE REPRESENTATION WITH FIDELITY AND CONSISTENCY

000
001
002
003
004
005 **Anonymous authors**
006 Paper under double-blind review
007
008
009
010
011
012
013
014
015
016
017
018
019
020
021
022
023
024
025
026
027
028
029
030
031
032
033
034
035
036
037
038
039
040
041
042
043
044
045
046
047
048
049
050
051
052
053

ABSTRACT

Representing symbolic, schema-diverse tables remains a fundamental challenge. Symbolic attributes often carry rich domain semantics, yet header formats and lexical expressions vary widely across tables, making it difficult for existing methods to maintain stable semantics. While language models capture semantic regularities, their token-level contextualization and sequential biases are misaligned with the bi-directional structure of tables, leading to sensitivity to schema and limited generalization across in-domain tables. Existing methods that seek to mitigate these limitations tend to favor either *fidelity*—preserving discriminative schema–value relationships—or *consistency*—maintaining robustness to lexical and structural variations—yet rarely achieving both. We argue that effective table representations must determine what should differ and what should remain the same across in-domain tables. To operationalize this principle, we introduce the header–value segment as a minimal, semantically coherent unit that captures both a header’s functional role and the domain semantics of its value. Figure 1 illustrates how segment-level modeling aligns domain-coherent schema variants while separating entity-specific content. Building on this idea, we propose NAVI—Entropy-aware Alignment with Header–Value Induction—a segment-centric framework that balances fidelity and consistency. Across real-world in-domain tables, NAVI significantly outperforms existing baselines on discriminative and generative tasks, while producing stable and interpretable segment embeddings. The source code of NAVI is available at: <https://anonymous.4open.science/r/navi>.

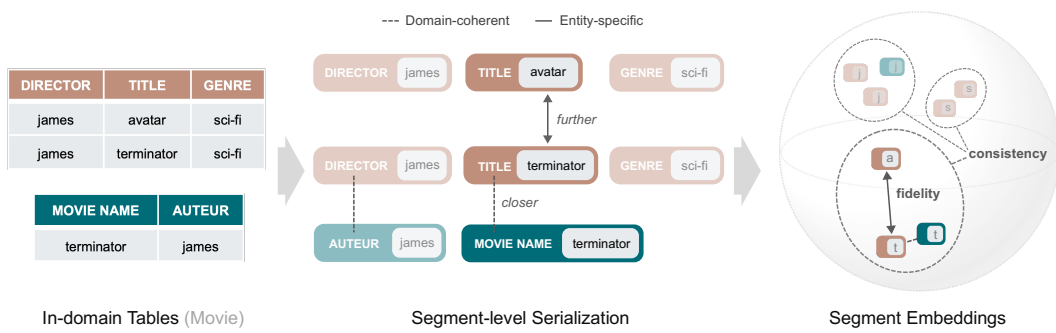


Figure 1: Illustration of **fidelity** and **consistency** in segment-level table representation. Left: In-domain movie tables exhibit heterogeneous schemas (e.g., DIRECTOR vs. AUTEUR) and symbolic attributes with shared domain semantics (e.g., GENRE). Middle: NAVI serializes each header–value pair into a *segment* and anchors headers using a global, context-free header encoder. Segments whose headers share similar semantics (e.g., DIRECTOR/AUTEUR or TITLE variants) are grouped accordingly, while segments containing different values under similar context (e.g., avatar vs. terminator) are also distinctly mapped. Right: After segment embedding, domain-coherent segments are pulled *closer* together, whereas entity-specific segments are pushed *further apart*. The figure visualizes how NAVI simultaneously enforces *consistency* (grouping lexical/structural variants) and *fidelity* (preserving discriminative entity-level semantics).

054

1 INTRODUCTION

055
Motivation. Tabular data encode information in a form fundamentally different from natural lan-
 056 guage. Headers instantiate domain-level semantics shared across rows and often across tables,
 057 yet they appear with substantial lexical noise, structural variation, and inconsistent formatting.
 058 While numerical attributes can be modeled reliably through type-aware techniques, symbolic at-
 059 tributes—categories, identifiers, and free-text values with widely varying cardinalities—carry much
 060 of a table’s semantic content and require richer representational modeling.
 061

062 Language models offer strong priors for symbolic data, but their sequential inductive biases make
 063 them ill-suited to the bi-directional layout of tables. They struggle with permutation invariance, het-
 064 erogeneous schema patterns, and stable relational semantics across tables, leading to unstable header
 065 representations, sensitivity to superficial schema changes, and entanglement between schema-level
 066 concepts and row-specific content; a detailed discussion follows in the next subsection.
 067

068 Classical pipelines such as gradient boosting decision trees Chen (2016) and numeric-specialized
 069 LM variants like TP-BERTa Yan et al. excel at capturing quantitative patterns, but they provide lim-
 070 ited leverage for modeling symbolic schema–value semantics or generalizing across heterogeneous
 071 table structures. Consequently, neither traditional tabular models nor existing LM-based encoders
 072 adequately address the representational needs of symbolic, schema-diverse in-domain tables.
 073

074 Overcoming these limitations requires preserving the semantic strengths of language models while
 075 correcting their structural blind spots. At the core is a fundamental question for table representa-
 076 tion learning: *what should differ, and what should remain the same across in-domain tables?* This
 077 distinction yields two complementary desiderata. **Fidelity** determines the aspects to which repre-
 078 sentations must remain sensitive—preserving functional roles (*structural fidelity*) and maintaining
 079 entity-level distinctions (*domain fidelity*). **Consistency** determines the invariances representations
 080 must maintain—robustness to schema perturbations (*structural consistency*) and stable domain se-
 081 mantics across heterogeneous tables (*domain consistency*).
 082

083 **Existing Works.** A large body of research adapts Transformer architectures to tabular data (Fang
 084 et al., 2024; Badaro et al., 2023), extending the success of sequence models on unstructured
 085 text (Vaswani et al., 2017; Devlin et al., 2019). These models serialize tables into token sequences
 086 and incorporate structural inductive biases—such as row/column embeddings or hierarchical encod-
 087 ings—to mitigate sequential biases. However, as in the typical trade-off between sensitivity and
 088 robustness in representation learning, existing methods struggle to achieve both *fidelity* and *consis-
 089 tency* simultaneously for in-domain tables.
 090

091 On the one hand, fidelity-oriented methods (Herzig et al., 2020; Yin et al., 2020; Iida et al., 2021;
 092 Deng et al., 2022; Wang et al., 2021) explicitly model rows, columns, or tree structures to capture
 093 fine-grained schema information of a table. By contextualizing tokens according to their functional
 094 roles in a table with vertical or horizontal attention, these methods achieve strong *fidelity*. However,
 095 they compromise the consistency of table representations; vulnerability to schema variations under-
 096 mines *structural consistency*, while table-specific designs hinder generalization across in-domain
 097 tables, weakening *domain consistency*.
 098

099 On the other hand, consistency-oriented methods (Jung & Yoon, 2025) enforce schema stability
 100 by interpolating context-free header embeddings with contextualized ones and regularizing their
 101 distance. Although this anchoring achieves *consistency*, it is applied only to header tokens and
 102 relies on token-level contextualization to absorb value information. As a result, the learned headers
 103 become largely value-independent, producing overly smoothed header semantics and a header–value
 104 misalignment that weakens both *structural* and *domain fidelity* under schema diversity.
 105

106 These limitations of existing methods fundamentally arise from the token-level contextualization of
 107 tabular data, similar to unstructured text, where table-specific adaptations function only as a lim-
 108 ited workaround. Merely token-level encoding fails to accurately learn header–value relationships,
 109 undermining fidelity, and to be fully aware of schema or lexical variation to preserve consistency.
 110

111 **Main idea and Contributions.** To bridge this gap, we introduce the concept of a header–value
 112 *segment*, a minimal yet semantically meaningful unit of a table that integrates structural roles with
 113 domain semantics. By treating the segment as the fundamental building block of representation
 114

learning, models can encode the essence of in-domain tables into a unified embedding that simultaneously balances fidelity and consistency. Grounded in this concept, we propose a novel tabular embedding framework **NAVI**: ENtropy-aware Alignment with Header-Value Induction. NAVI aims to capture the structural properties of tables through *schema-aware segment induction and modeling*. It also employs *entropy-driven alignment of segments* to selectively incorporate domain knowledge shared among in-domain tables.

In summary, we make the following contributions: (1) We identify the two key desiderata, fidelity and consistency, as a principled foundation for effective in-domain table representation learning. (2) We introduce the notion of a header-value segment as the fundamental building block of tables, and propose NAVI, a novel segment-centric embedding framework, with a theoretical analysis for the two desiderata. (3) We conduct extensive experiments on real-world in-domain tables, showing that NAVI outperforms existing baselines in both discriminative and generative downstream tasks. In addition, qualitative analyses further demonstrate the effectiveness of NAVI.

2 METHODOLOGY

We present a three-stage framework for segment-grounded representation learning from tabular data. Our methodology consists of: (1) Schema-aware Segment Induction, which defines the header–value segment as a structural unit and incorporates context-free header embeddings to ensure structural consistency; (2) Masked Segment Modeling, which extends the masked language modeling (MLM) objective with balanced masking of headers and values to enforce fine-grained schema–value dependencies, thereby achieving structural fidelity; and (3) Entropy-driven Segment Alignment, which leverages column entropy to distinguish domain-defining from entity-defining attributes, applying cross-column and cross-row alignment to ensure domain consistency and domain fidelity.

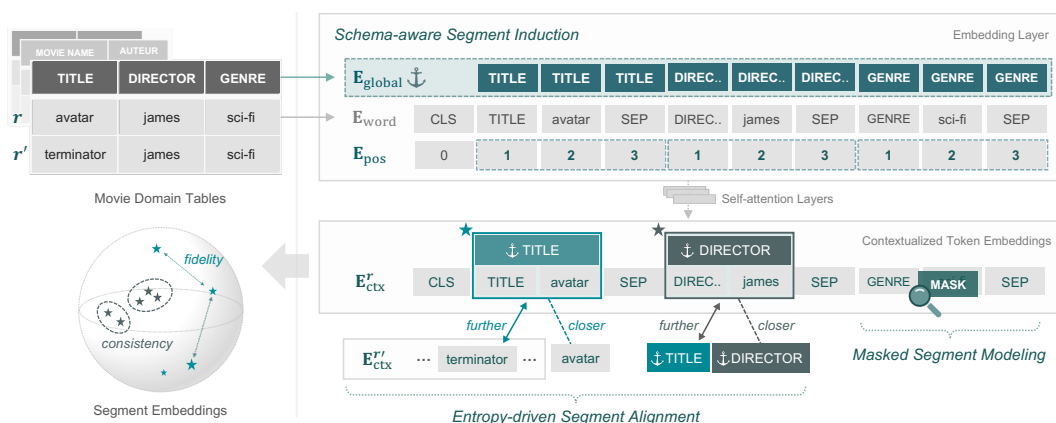


Figure 2: Overall procedure of NAVI. We optimize schema-induced representations for tokens and segments with masked modeling and entropy-driven alignment, preserving intra-table fidelity and inter-table consistency for in-domain tables.

2.1 SCHEMA-AWARE SEGMENT INDUCTION

Header-Value Segment. Unlike natural language, tables are inherently organized into rows, each corresponding to a distinct entity. To preserve this entity-level semantics while avoiding spurious cross-row interactions, we serialize each row independently as an unordered set of *header–value segments*. Each segment is constructed in the canonical form *header : value* [SEP] with a special [CLS] token prefixed at the row level. This segmentation provides an explicit structural unit that grounds schema semantics without imposing any ordering among columns.

For each segment, we identify header-token indices and value-token indices based on the tokenized sequence, excluding delimiter and special tokens. For example:

162
163
164
165

In the resulting token sequence, header tokens form the header span $\mathcal{P}_{\text{MOVIE NAME}} = [1, 2]$, while value tokens form the value span $\mathcal{P}_{\text{harrypotter}} = [4, 5]$. The delimiter ":" is treated as a boundary marker and is omitted from both spans, and special tokens are likewise excluded. To prevent the model from encoding column order, each segment k of length m_k is assigned an independent positional reinitialization:

171
172
173
174

$$E_{\text{pos}}(x_j^{(k)}) = P_j, \quad j = 0, \dots, m_k - 1,$$

where P_j is a sinusoidal positional embedding. This yields both row and column permutation invariance, and together these invariances constitute the form of *structural consistency*.

175
176
177
178
179
180
181
182
183
184
185

Global Header Representation. To anchor header semantics consistently across contexts (e.g., rows, tables), we introduce a lightweight encoder dedicated for encoding header strings. Given a header tokenized as $h = [t_1, \dots, t_n]$, the encoder produces self-attended embeddings $\{e_{t_1}, \dots, e_{t_n}\}$, $e_{t_k} \in \mathbb{R}^d$. A single universal embedding for header h , $E_{\text{global}}(h) \in \mathbb{R}^d$ is then obtained by pooling, independent of any specific table context.

Unlike prior approaches that construct column embeddings by coupling headers with local values (Yin et al., 2020; Iida et al., 2021), our header representations remain context-free. This provides a consistent semantic anchor across diverse tables and serves as a supportive bias for domain consistency. It is further complemented by stronger distribution-level regularization through entropy-driven segment alignment.

186
187
188
189

Header-conditioned Token Representation. To provide a supportive bias toward domain-level consistency, we condition token embeddings on their corresponding global header representations. Specifically, $E_{\text{global}}(h)$ is added as a bias to each token $x_j^{(k)}$ within its segment:

$$z_j^{(k)} = E_{\text{word}}(x_j^{(k)}) + E_{\text{pos}}(x_j^{(k)}) + E_{\text{global}}(h_k).$$

These conditioned embeddings are contextualized by a transformer encoder, yielding token representations $\mathbf{e}_t \in \mathbb{R}^d$. This mechanism enforces a stable schema bias, promoting *structural fidelity* by maintaining schema-value dependencies under noisy or mutated tables.

Building on this token representation, we obtain header- and value-level contextual embeddings by mean-pooling the encoder outputs at their respective spans. The contextualized header embedding $H_{\text{ctx}}(r, h)$ is obtained by pooling over positions in \mathcal{P}_h , and the contextualized value embedding $V_{\text{ctx}}(r, h)$ is analogously obtained from positions in \mathcal{P}_v . These span-based contextual embeddings preserve the intended structural separation between schema and content while capturing their interactions within each row.

200

Header-conditioned Segment Representation. At the row level, we construct segment embeddings that integrate both schema anchors and contextualized representations. For header h in row r , we first obtain contextualized token embeddings from the transformer encoder output. The contextualized header and value embeddings, respectively denoted as $H_{\text{ctx}}(r, h)$ and $V_{\text{ctx}}(r, h)$, are extracted by pooling the contextualized token embeddings at the positions of h and its corresponding value.

Finally, the segment embedding concatenates the global header with row-aware components:

207
208

$$E_{\text{seg}}(r, h) = g(E_{\text{global}}(h) \parallel H_{\text{ctx}}(r, h) \parallel V_{\text{ctx}}(r, h)),$$

where \parallel denotes concatenation, and $g(\cdot)$ is a projection network. Such integrated embeddings capture both schema–value dependencies and global semantics, thereby providing a relationally expressive foundation that promotes *domain fidelity* across heterogeneous tables.

212
213
214

2.2 MASKED SEGMENT MODELING

215

Structure-based Masking. Standard masked language modeling (MLM) has proven effective for natural language (Devlin et al., 2019), but its direct application to tables is suboptimal. Headers

and values are semantically different, and their dependencies are crucial for relational reasoning. By treating all tokens uniformly, Vanilla MLM risks overlooking the structural distinction between schema and content, undermining its ability to maintain *structural fidelity*. To address this, we introduce a structure-aware masked segment modeling (MSM) that explicitly models schema–value dependencies by partitioning each row of segments into three masking regimes:

- **Header-masked segments:** header tokens in selected segments are masked, forming the set \mathcal{M}_h . The model must recover header names from associated values.
- **Value-masked segments:** value tokens in selected segments are masked, forming the set \mathcal{M}_v . The model must infer values from headers and row context.
- **Vanilla MLM:** a random subset of remaining tokens is masked, forming \mathcal{M}_r . This acts as a regularization term that prevents overfitting to header–value co-occurrence patterns.

Objective. For each masked token $t \in \mathcal{M}$ with contextualized token embedding \mathbf{e}_t , the classifier produces a logit vector $\mathbf{z}_t = W\mathbf{e}_t + b \in \mathbb{R}^{|\mathcal{V}|}$. The masked segment modeling (MSM) loss is then given by the standard softmax cross-entropy:

$$\mathcal{L}_{\text{msm}} = -\frac{1}{|\mathcal{M}|} \sum_{t \in \mathcal{M}} \log \frac{\exp(\mathbf{z}_t[t])}{\sum_{v \in \mathcal{V}} \exp(\mathbf{z}_t[v])}, \quad \mathcal{M} = \mathcal{M}_h \cup \mathcal{M}_v \cup \mathcal{M}_r,$$

where $\mathbf{z}_t[v]$ is the logit corresponding to vocabulary item v . The MSM objective with structured masking compels the encoder to learn functional roles of tokens and schema–value dependencies, thereby realizing the *structural fidelity*.

2.3 ENTROPY-DRIVEN SEGMENT ALIGNMENT

Entropy-based Column Categorization. While the preceding methods ensure structural consistency and structural fidelity, they do not by themselves guarantee domain consistency or domain fidelity. To achieve these desiderata, we require an additional mechanism that explicitly aligns representations. Contrastive learning (Oord et al., 2018; Chen et al., 2020; Lee et al., 2022) has been widely used to arrange embeddings according to a target semantic objective, but the straightforward adoption—applying contrastive loss directly at the row (i.e., instance, entity) level—fails to distinguish between schema-level semantics and instance-specific attributes. This results in entangled representations that blur domain boundaries or collapse row-level distinctions.

To overcome this limitation, we propose an entropy-based column categorization. Instead of aligning rows indiscriminately, we categorize columns by the entropy of their empirical value distributions and use this categorization as the foundation for aligning segments and headers-values:

- **Domain-coherent columns \mathcal{H}_{dom} :** low-entropy columns (e.g., below the **10 percentile**) with stable domain-level concepts (e.g., genre and director in movie tables). Aligning their segments and headers enforces consistent semantics across tables, promoting *domain consistency*.
- **Entity-discriminative columns \mathcal{H}_{ent} :** high-entropy columns (e.g., above the **90 percentile**) with instance-specific attributes (e.g., title and url in movie tables). Aligning their segments and values enhances row separability within a domain, enhancing *domain fidelity*.

Objective. Given a query q , a positive sample x^+ , a set of negative samples \mathcal{X}^- , and a temperature τ , the InfoNCE objective (Oord et al., 2018) is set as:

$$\mathcal{L}_{\text{InfoNCE}}(q, x^+, \mathcal{X}^-, \tau) = -\log \frac{\exp(q \cdot x^+ / \tau)}{\exp(q \cdot x^+ / \tau) + \sum_{x^- \in \mathcal{X}^-} \exp(q \cdot x^- / \tau)}.$$

For headers in domain-coherent columns $h_{\text{dom}} \in \mathcal{H}_{\text{dom}}$, cross-header alignment matches segments with their global header embeddings. This ensures that headers representing similar domain concepts are consistently aligned across rows and tables. We optimize the domain-coherent loss:

$$\mathcal{L}_{\text{dom}}^t = \mathbb{E}_{r \sim \mathcal{R}, h \sim \mathcal{H}_{\text{dom}}} [\mathcal{L}_{\text{InfoNCE}}(q_{\text{dom}}(r, h), x_{\text{dom}}^+(h), \mathcal{X}_{\text{dom}}^-(h), \tau_{\text{dom}})], \text{ where}$$

$$q_{\text{dom}}(r, h) = E_{\text{seg}}(r, h), \quad x_{\text{dom}}^+(h) = E_{\text{global}}(h), \quad \mathcal{X}_{\text{dom}}^-(h') = \{ E_{\text{global}}(h') \mid h' \in \mathcal{H}_{\text{dom}}, h' \neq h \}.$$

270 For headers in entity-discriminative columns $h_{\text{ent}} \in \mathcal{H}_{\text{ent}}$, cross-row alignment matches segments
 271 with row-aware values. This encourages row-level separability by ensuring distinct rows in the
 272 same table remain distinguishable. We optimize the entity-discriminative loss:

$$273 \quad \mathcal{L}_{\text{ent}}^t = \mathbb{E}_{r \sim \mathcal{R}, h \sim \mathcal{H}_{\text{ent}}} [\mathcal{L}_{\text{InfoNCE}}(q_{\text{ent}}(r, h), x_{\text{ent}}^+(h), \mathcal{X}_{\text{ent}}^-(h), \tau_{\text{ent}})], \text{ where} \\ 274 \quad q_{\text{ent}}(r, h) = E_{\text{seg}}(r, h), x_{\text{ent}}^+(r, h) = V_{\text{ctx}}(r, h), \mathcal{X}_{\text{ent}}^-(r, h) = \{V_{\text{ctx}}(r', h) \mid r' \in \mathcal{R}, r' \neq r\}.$$

277 Finally, given a batch \mathcal{B} in input tables and a balancing parameter λ_{align} for generative and discriminative
 278 supervision, the overall training objective is formulated as:

$$280 \quad \mathcal{L}_{\text{total}} = \mathcal{L}_{\text{msm}} + \lambda_{\text{align}} \cdot \mathcal{L}_{\text{align}}, \text{ where } \mathcal{L}_{\text{align}} = 1/|\mathcal{B}| \cdot \sum_{t \in \mathcal{B}} (\mathcal{L}_{\text{dom}}^t + \mathcal{L}_{\text{ent}}^t).$$

283 Appendix A discusses the theoretical analysis of the schema induction and contrastive alignment.

285 3 EXPERIMENTS

288 3.1 EXPERIMENTAL SETUP

289 **Datasets.** We evaluate on four datasets from two domains, Movie and Product. For pretraining,
 290 we use subsets of WDC WebTables (Peeters et al., 2024), selecting the 100 largest tables per do-
 291 main—WDC Movie (480,817 rows) and WDC Product (3,930,877 rows)—and subsample 480,817
 292 rows from each for balance. To ensure compatibility with BERT-style models, all tables are pro-
 293 cessed through a standardized pipeline (see Appendix D.2). For downstream evaluation, we con-
 294 struct held-out subsets of 45,000 rows per domain ($\approx 10\%$ of pretraining). We uniformly subsample
 295 1,000 rows per each evaluation run for consistency and efficiency.

296 **Baseline Methods.** We evaluate our approach against representative table embedding models span-
 297 ning major paradigms. BERT serves as the generic transformer backbone underlying most language
 298 model-based table encoders; its performance highlights the limitations of applying vanilla language
 299 models to tabular data. TAPAS, the most widely adopted table encoder, exemplifies fidelity-oriented
 300 approaches, while HAETAЕ represents a consistency-oriented encoder. This selection enables a
 301 systematic comparison of their strengths and limitations with respect to fidelity and consistency.

302 **Implementaion.** We configure NAVI to balance domain and structural objectives. For domain
 303 objectives, we set contrastive temperature τ to **0.02** for entity-discriminative columns and **0.14** for
 304 domain-coherent columns, and vary the alignment weight λ_{align} across tasks. For structural objec-
 305 tives, we adjust the header–value–baseline (H:V:B) masking ratio. We use λ_{align} as **0.05** and H:V:B
 306 = 4:4:2 as the default. Further details and sensitivity analysis appear in Appendix D. All models are
 307 trained on the same datasets for 2 epochs with a batch size of 32, AdamW (Loshchilov & Hutter)
 308 with a learning rate of 3×10^{-5} , and a weight decay of 0.01.

310 3.2 FIDELITY ANALYSIS

311 We evaluate *fidelity*, the faithfulness of representations to table semantics. Fidelity spans two dimen-
 312 sions: *domain fidelity*, which preserves entity-level discriminability, and *structural fidelity*, which
 313 models schema–value dependencies within rows. We probe domain fidelity through **discrimina-**
 314 **tive tasks** (Row Classification and Row Clustering) and structural fidelity through **generative tasks**
 315 (Value Imputation and Header Prediction).

317 **Discriminative Tasks.** To assess *domain fidelity*—whether embeddings preserve entity-level
 318 separability—we evaluate *Row Classification* and *Row Clustering*. For **LM-based table encoders**
 319 (**BERT**, **TAPAS**, **HAETAЕ**, and **NAVI**), each row is serialized and encoded once; the final **[CLS]**
 320 embedding is used as a feature vector for downstream evaluation. Classification uses **10** balanced
 321 classes per domain (top product categories, top movie genres; $\sim 1,000$ samples), reporting Macro-
 322 F1 from XGBoost, Logistic Regression, and TabPFN. Clustering probes the same label space via
 323 Agglomerative, scored by Silhouette and **B³-F1**, with all results averaged over **5** subsampled runs.
 As shown in Table 1, BERT relies on shallow cues and achieves modest discriminability, while

Table 1: Performance on discriminative tasks. The table shows results from [CLS] token embeddings. Macro-F1 scores for classification (using XGBoost, Logistic Regression, TabPFN) and Silhouette and B³-F1 scores for clustering (using Agglomerative).

Model	Product				Movie			
	R-Cls (F1)			R-Clt (Sil/ B ³)	R-Cls (F1)			R-Clt (Sil/ B ³)
	XGB	LR	PFN	Agglo.	XGB	LR	PFN	Agglo.
BERT	0.915	0.931	0.938	0.215 / 0.605	0.597	0.653	0.647	0.076 / 0.274
TAPAS	0.927	0.934	0.932	0.406 / 0.770	0.607	0.665	0.675	0.087 / 0.320
HAETAE	0.916	0.942	0.938	0.233 / 0.663	0.607	0.634	0.663	0.073 / 0.279
NAVI	0.930	0.941	0.945	0.424 / 0.833	0.639	0.667	0.670	0.100 / 0.297
Raw	0.888	0.780	0.882	— / —	0.464	0.415	0.498	— / —
TableVectorizer	0.933	0.909	0.940	— / —	0.618	0.540	N/A	— / —
NAVI _{text_emb+num}	0.942	0.941	0.943	— / —	0.641	0.658	0.669	— / —

HAETAE’s rigid anchoring suppresses value-sensitive variation. TAPAS improves fidelity but remains schema-sensitive. By contrast, NAVI consistently leads across classifiers and clustering, yielding compact and coherent row manifolds—demonstrating that entropy-driven alignment mitigates row collapse and strengthens entity-level fidelity under schema diversity.

Beyond LM-based encoders, we also evaluate non-LM baselines on the classification task—namely raw-feature classifiers (XGBoost, Logistic Regression, TabPFN) and TableVectorizer. TableVectorizer is a type-aware feature-engineering pipeline that scales numeric fields, encodes temporal attributes, applies one-hot encoding to low-cardinality text, and uses SentenceTransformer embeddings for high-cardinality text. Although powerful, this design produces very high-dimensional vectors in text-heavy domains such as Movie (often exceeding 2,000 dimensions), making it incompatible with TabPFN (N/A) and substantially larger than NAVI’s 768-dimensional embeddings—yet without surpassing NAVI. This suggests that NAVI’s performance could further improve with more complex encoder backbones Warner et al. (2025).

At the same time, TableVectorizer’s strong performance demonstrates the value of type-aware feature engineering, particularly its explicit handling of numerical and temporal fields. Its main limitation lies in relying on a generic natural-language encoder (SentenceTransformer) for high-cardinality text. Replacing this component with a table-specialized LM encoder is therefore a promising direction. We illustrate this with a simple hybrid prototype, NAVI_{text_emb+num}, which concatenates raw numerical features with NAVI’s text-derived segments and already surpasses both raw-feature and the TableVectorizer pipeline. This indicates that NAVI can serve as a drop-in replacement for generic text encoders in feature-engineering pipelines, potentially yielding even stronger performance.

Generative Tasks. We examine *structural fidelity*, i.e., whether embeddings capture schema–value dependencies, through two tasks: *Header Prediction* and *Value Imputation*, respectively recovering masked headers and values from contextualized row tokens. We compare NAVI against BERT and HAETAE, which are naturally suited for generative tasks, but exclude TAPAS as its QA-oriented pretraining objective makes it infeasible for this setting. As shown in Table 2, NAVI achieves near-perfect header prediction, validating its global header encoder as a stable semantic anchor, and also outperforms in value imputation, where header-conditioned representations and structure-aware masking reinforce schema–value dependencies.

Table 2: Generative tasks.

Model	Product	Movie
<i>Header</i>		
BERT	<u>0.9284</u>	<u>0.9159</u>
HAETAE	0.9219	0.9120
NAVI	0.9995	0.9990
<i>Value</i>		
BERT	0.7586	0.6809
HAETAE	<u>0.7735</u>	<u>0.6879</u>
NAVI	0.7902	0.7077

3.3 CONSISTENCY ANALYSIS

We next evaluate *consistency*, the stability of representations under schema diversity. Consistency has two dimensions: *domain consistency* and *structural consistency*, which together denote invariance to lexical and structural diversity. Domain consistency is measured by clustering semantically

equivalent headers (e.g., `director` vs. `auteur`) using agglomerative clustering, with quality assessed by B^3 -F1 and NMI. Structural consistency is measured by permuting rows and computing the permutation sensitivity index ($PSI = \mathbb{E}_k[1 - \cos(z, \tilde{z}^{(k)})]$), where z is the original row embedding and $\tilde{z}^{(k)}$ its k -th permutation, using both CLS and mean pooling. Consistent models should form compact header clusters and yield low PSI.

Table 3: Domain consistency of header clustering (H-Clt) is evaluated by B^3 -F1 and NMI (higher is better), and structural consistency of row permutation is evaluated with PSI (lower is better).

Model	Product		Movie	
	H-Clt (B^3 -F1 / NMI)	PSI (cls / mean)	H-Clt (B^3 -F1 / NMI)	PSI (cls / mean)
BERT	0.7317 / 0.8749	6.35 e-2 / 7.59 e-3	0.6969 / 0.8798	5.81 e-2 / 6.61 e-3
TAPAS	0.7239 / 0.8750	1.24 e-2 / 6.70 e-3	0.6759 / 0.8726	1.01 e-2 / 6.32 e-3
HAETAE	0.7268 / 0.8742	6.15 e-2 / 8.70 e-3	0.7276 / 0.8864	6.53 e-2 / 7.83 e-3
NAVI	0.7920 / 0.9005	9.55 e-8 / 1.97 e-8	0.7996 / 0.9144	1.15 e-6 / 1.96 e-8

Lexical Diversity. On header clustering, NAVI yields the most coherent groups. HAETAE is competitive but still weaker than NAVI’s alignment. Figure 3 illustrates this for the `actor` set: under NAVI (top), lexical variants converge into one cluster, while under BERT (bottom) they remain split. This contrast shows BERT encodes surface forms, whereas NAVI collapses aliases into canonical representations. Thus, the induction with contrastive alignment enforces domain consistency.

Structural Diversity. As shown in Table 3, BERT and HAETAE exhibit high PSI, indicating that their row representations remain sensitive to positional or ordering artifacts. TAPAS reduces this sensitivity but still preserves measurable permutation effects. In contrast, NAVI yields PSI values that are one to two orders of magnitude lower, approaching true invariance to row permutations. This shows that schema induction suppress spurious structural cues, producing stable row embeddings.

3.4 ABLATION STUDY

To disentangle the contribution of each component in NAVI, we organize our analysis along the four desiderata of our evaluation framework. On the fidelity side, we assess *domain fidelity* with Row Classification (R-Cls) and *structural fidelity* with Value Imputation (Val). On the consistency side, we measure *domain consistency* with Header Clustering (H-Clt) and *structural consistency* with the Permutation Sensitivity Index (PSI). This one-to-one mapping provides a clear lens into how Schema-aware Segment Induction (SSI), Structure-aware MSM (SMSM), and Entropy-driven Segment Alignment (ESA) each contribute to representations that are both faithful and consistent.

Table 4: Classification (Logistic Regression - F1), Accuracy for Value Imputation, Header Clustering (Agglomerative - NMI), Permutation Sensitivity Index (computed from `cls` row embeddings) across Product and Movie domains.

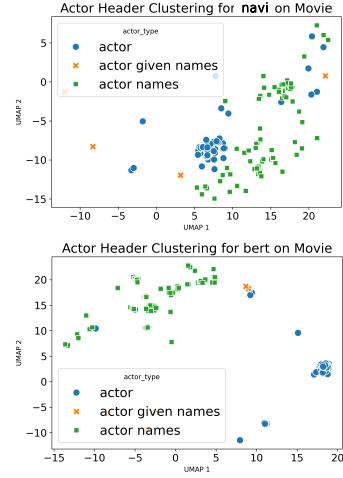


Figure 3: Header embeddings.

Variant	Product				Movie			
	R-Cls	Val	H-Clt	PSI	R-Cls	Val	H-Clt	PSI
NAVI	0.9412	0.7902	0.9005	9.55e-8	0.6670	0.7077	0.9144	1.15e-8
w/o SSI	0.9137	0.2627	0.7071	1.35e-7	0.4899	0.2522	0.4374	1.52e-7
w/o MSM	0.9091	0.7659	0.8989	2.45e-7	0.5790	0.6927	0.9018	9.63e-8
w/o ESA	0.9358	0.7897	0.9007	1.92e-7	0.6488	0.7086	0.9149	9.26e-8

432 Results in Table 4 clarify how each module of NAVI sustains our four desiderata. Removing SSI
 433 yields the most severe degradation, collapsing Value Imputation and Header Clustering, which con-
 434 firms schema anchoring as the linchpin of both fidelity and consistency. Removing MSM primarily
 435 affects structural fidelity and domain fidelity: value imputation and row classification drop, but
 436 consistency metrics (H-Clt, PSI) remain relatively stable, confirming that structure-aware masking
 437 mainly supervises schema–value functional roles rather than cross-table alignment. Dropping ESA
 438 leads to a clear loss in domain fidelity ($R\text{-}Cls$ 0.9412 → 0.9358; 0.6670 → 0.6488), while the small
 439 gains in consistency are effectively negligible (H-Clt 0.9005 → 0.9007; 0.9144 → 0.9149). This shows
 440 that ESA plays a decisive role in enhancing row-level discrimination and preserving entity-specific
 441 distinctions. Overall, SSI provides the consistent structural backbone, MSM enforces structural
 442 fidelity, and ESA substantially strengthens domain fidelity.

443

444

445

446 3.5 QUALITATIVE ANALYSIS

447

448

449 Figure 4 visualizes segment embeddings from BERT and
 450 NAVI, both trained on the Movie domain. For BERT, segment
 451 embeddings are constructed by mean-pooling the contextualized
 452 token embeddings of each header–value span, ensuring
 453 comparability with NAVI’s segment-level outputs. We project
 454 the resulting embeddings using t-SNE.

455

456 The geometry of BERT’s segment space reflects the absence
 457 of explicit header–value alignment. Although high- and low-
 458 entropy segments appear almost linearly separable, their inter-
 459 nal organization lacks meaningful semantic structure. Low-
 460 entropy segments—those expected to encode stable, domain-
 461 level concepts—scatter across the space with inconsistent
 462 shapes and densities, suggesting that BERT fails to form co-
 463 herent semantic anchors. This instability is consistent with our
 464 hypothesis that contextual embeddings conflate schema-level
 465 semantics with row-specific fluctuations.

466

467 High-entropy segments, which should preserve fine-grained
 468 row identity, instead fragment into numerous compact, table-
 469 specific micro-clusters driven by superficial lexical or struc-
 470 tural cues. Consequently, these segments become entangled
 471 with table-conditioned schematic patterns rather than main-
 472 taining consistent entity representations across tables. This
 473 behavior reflects the lack of domain fidelity: segments repre-
 474 senting distinct rows are pulled together or separated in ways
 475 that mirror table artifacts rather than underlying semantics.

476

477 In contrast, NAVI induces a markedly different and more principled structure, shaped by its entropy-
 478 driven segment alignment objective. Low-entropy segments concentrate into tight, well-localized
 479 clusters that function as domain anchors. These clusters reflect NAVI’s cross-header alignment for
 480 domain-coherent columns, where global header embeddings act as stable semantic centroids. The
 481 resulting contraction toward these centroids demonstrates that NAVI successfully extracts consistent
 482 schema-level semantics while filtering out table-specific noise.

483

484 High-entropy segments—aligned through row-level contrastive signals rather than schema-level in-
 485 duction—exhibit broader, more dispersed clusters. Instead of collapsing or fragmenting by table
 486 identity, they maintain coarse separation while remaining grounded in the shared domain space.
 487 This behavior arises because high-entropy alignment is anchored to each specific column: segments
 488 repel one another to preserve row-level distinctiveness, yet do not drift away from the semantic man-
 489 ifold defined by the domain. Importantly, these clusters do not collapse even when similar contextual
 490 patterns occur within the same table, illustrating NAVI’s ability to preserve instance-level variability
 491 without overfitting to table-specific quirks.

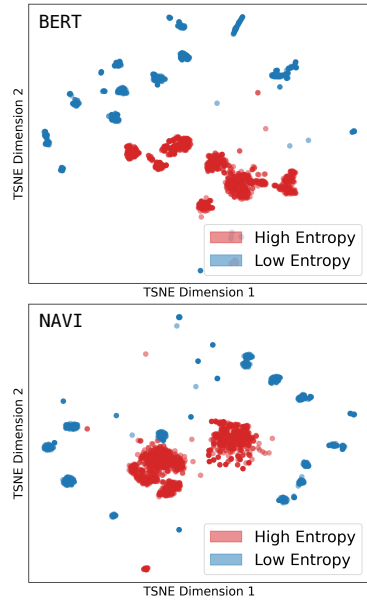


Figure 4: Visualization of segment embeddings from five heterogeneous Movie tables.

486 4 CONCLUSION
487

488 In this paper, we revisit table representation through the two principled desiderata, fidelity and
489 consistency, and exploit the header–value segment as the atomic unit to balance them. NAVI implements
490 this idea with (i) Schema-aware Segment Induction (SSI) that builds segment embeddings anchored
491 by a global, context-free header encoder, (ii) Masked Segment Modeling (MSM) that enforces fine-
492 grained schema–value dependencies, and (iii) Entropy-driven Segment Alignment (ESA) that aligns
493 domain-coherent columns while preserving separation for entity-discriminative ones. Empirical
494 studies demonstrated that NAVI achieves higher performances on both header prediction and value
495 imputation, in addition to consistent gains on classification and clustering tasks. Qualitatively, the
496 resulting embedding space exhibits a core–periphery geometry (i.e., a shared semantic core for sta-
497 ble headers and a flexible periphery for instance-specific attributes) in accordance with our learning
498 objectives. Ablation studies also confirm that the efficacy of the three main components: SSI as the
499 building blocks for fidelity and consistency, MSM for schema–value coupling, and ESA for permu-
500 tation stability and row discriminability. Together, these results position NAVI as a segment-centric,
501 alignment-guided alternative to existing token-oriented encoders, narrowing the gap between sym-
502 bolic tabular data and contextualized representations. We believe this work opens up practical oppor-
503 tunities and future work for applications with LLM-table interactions, such as question answering
504 and retrieval-augmented generation on in-domain tables.

505 REFERENCES
506

507 Jimmy Lei Ba, Jamie Ryan Kiros, and Geoffrey E Hinton. Layer normalization. *arXiv preprint
arXiv:1607.06450*, 2016.

509 Gilbert Badaro, Mohammed Saeed, and Paolo Papotti. Transformers for tabular data representa-
510 tion: A survey of models and applications. *Transactions of the Association for Computational
511 Linguistics*, 2023.

513 Tianqi Chen. Xgboost: A scalable tree boosting system. *Cornell University*, 2016.

514 Ting Chen, Simon Kornblith, Mohammad Norouzi, and Geoffrey Hinton. A simple framework for
515 contrastive learning of visual representations. In *International conference on machine learning*,
516 pp. 1597–1607. PMLR, 2020.

518 Kevin Clark, Urvashi Khandelwal, Omer Levy, and Christopher D. Manning. What does BERT look
519 at? an analysis of BERT’s attention. In Tal Linzen, Grzegorz Chrupała, Yonatan Belinkov, and
520 Dieuwke Hupkes (eds.), *Proceedings of the 2019 ACL Workshop BlackboxNLP: Analyzing and
521 Interpreting Neural Networks for NLP*, pp. 276–286, Florence, Italy, August 2019. Association
522 for Computational Linguistics. doi: 10.18653/v1/W19-4828.

523 Xiang Deng, Huan Sun, Alyssa Lees, You Wu, and Cong Yu. Turl: Table understanding through
524 representation learning. *ACM SIGMOD Record*, 51(1):33–40, 2022.

526 Jacob Devlin, Ming-Wei Chang, Kenton Lee, and Kristina Toutanova. BERT: Pre-training of deep
527 bidirectional transformers for language understanding. In *Proceedings of the 2019 Conference of
528 the North American Chapter of the Association for Computational Linguistics: Human Language
529 Technologies*, 2019.

530 Xi Fang, Weijie Xu, Fiona Anting Tan, Jian Zhang, Ziqing Hu, Yanjun Qi, Scott Nickleach, Diego
531 Socolinsky, Srinivasan Sengamedu, and Christos Faloutsos. Large language models on tabu-
532 lar data: Prediction, generation, and understanding—a survey. *arXiv preprint arXiv:2402.17944*,
533 2024.

534 Jonathan Herzig, Paweł Krzysztof Nowak, Thomas Müller, Francesco Piccinno, and Julian Eisen-
535 schlos. TaPas: Weakly supervised table parsing via pre-training. In *Proceedings of the 58th
536 Annual Meeting of the Association for Computational Linguistics*, 2020.

538 Noah Hollmann, Samuel Müller, Katharina Eggensperger, and Frank Hutter. Tabpfn: A transformer
539 that solves small tabular classification problems in a second. In *NeurIPS 2022 First Table Repre-
540 sentation Workshop*.

540 Hiroshi Iida, Dung Thai, Varun Manjunatha, and Mohit Iyyer. Tabbie: Pretrained representations of
 541 tabular data. *arXiv preprint arXiv:2105.02584*, 2021.

542

543 Woojun Jung and Susik Yoon. HAETAE: In-domain table pretraining with header anchoring. In
 544 *Proceedings of the 48th International ACM SIGIR Conference on Research and Development in*
 545 *Information Retrieval*, pp. 3065–3069, 2025.

546

547 Janghyeon Lee, Jongsuk Kim, Hyounguk Shon, Bumsoo Kim, Seung Hwan Kim, Honglak Lee, and
 548 Junmo Kim. Uniclip: Unified framework for contrastive language-image pre-training. *Advances*
 549 *in Neural Information Processing Systems*, 35:1008–1019, 2022.

550

551 Peng Li, Yeye He, Dror Yashar, Weiwei Cui, Song Ge, Haidong Zhang, Danielle Rifinski Fainman,
 552 Dongmei Zhang, and Surajit Chaudhuri. Table-GPT: Table fine-tuned gpt for diverse table tasks.
 553 2024.

554

555 Qian Liu, Bei Chen, Jiaqi Guo, Morteza Ziyadi, Zeqi Lin, Weizhu Chen, and Jian-Guang Lou.
 556 Tapex: Table pre-training via learning a neural sql executor. In *International Conference on*
 557 *Learning Representations*.

558

559 Ilya Loshchilov and Frank Hutter. Decoupled weight decay regularization. In *International Conference*
 560 *on Learning Representations*.

561

562 Markus Mueller, Kathrin Gruber, and Dennis Fok. Continuous diffusion for mixed-type tabular data.
 563 *arXiv preprint arXiv:2312.10431*, 2023.

564

565 Aaron van den Oord, Yazhe Li, and Oriol Vinyals. Representation learning with contrastive predic-
 566 tive coding. *arXiv preprint arXiv:1807.03748*, 2018.

567

568 Ralph Peeters, Alexander Brinkmann, and Christian Bizer. The web data commons schema.org table
 569 corpora. In *Companion Proceedings of the ACM Web Conference 2024*, 2024.

570

571 Nikunj Saunshi, Orestis Plevrakis, Sanjeev Arora, Mikhail Khodak, and Hrishikesh Khandeparkar.
 572 A theoretical analysis of contrastive unsupervised representation learning. In *International con-*
 573 *ference on machine learning*, pp. 5628–5637. PMLR, 2019.

574

575 Ashish Vaswani, Noam Shazeer, Niki Parmar, Jakob Uszkoreit, Llion Jones, Aidan N Gomez,
 576 Łukasz Kaiser, and Illia Polosukhin. Attention is all you need. *Advances in neural informa-*
 577 *tion processing systems*, 30, 2017.

578

579 Tongzhou Wang and Phillip Isola. Understanding contrastive representation learning through align-
 580 ment and uniformity on the hypersphere. In *International conference on machine learning*, pp.
 581 9929–9939. PMLR, 2020.

582

583 Zhiruo Wang, Haoyu Dong, Ran Jia, Jia Li, Zhiyi Fu, Shi Han, and Dongmei Zhang. Tuta: Tree-
 584 based transformers for generally structured table pre-training. In *Proceedings of the 27th ACM*
 585 *SIGKDD Conference on Knowledge Discovery & Data Mining*, pp. 1780–1790, 2021.

586

587 Benjamin Warner, Antoine Chaffin, Benjamin Clavié, Orion Weller, Oskar Hallström, Said
 588 Taghadouini, Alexis Gallagher, Raja Biswas, Faisal Ladhak, Tom Aarsen, et al. Smarter, bet-
 589 ter, faster, longer: A modern bidirectional encoder for fast, memory efficient, and long context
 590 finetuning and inference. In *Proceedings of the 63rd Annual Meeting of the Association for Com-*
 591 *putational Linguistics (Volume 1: Long Papers)*, pp. 2526–2547, 2025.

592

593 Jiahuan Yan, Bo Zheng, Hongxia Xu, Yiheng Zhu, Danny Z Chen, Jimeng Sun, Jian Wu, and Jintai
 594 Chen. Making pre-trained language models great on tabular prediction.

595

596 Pengcheng Yin, Graham Neubig, Wen-tau Yih, and Sebastian Riedel. TaBERT: Pretraining for joint
 597 understanding of textual and tabular data. In *Proceedings of the 58th Annual Meeting of the*
 598 *Association for Computational Linguistics*, 2020.

599

600 Manzil Zaheer, Satwik Kottur, Siamak Ravanbakhsh, Barnabas Poczos, Russ R Salakhutdinov, and
 601 Alexander J Smola. Deep sets. *Advances in neural information processing systems*, 30, 2017.

594 Yilun Zhao, Lyuhao Chen, Arman Cohan, and Chen Zhao. Tapera: enhancing faithfulness and
595 interpretability in long-form table qa by content planning and execution-based reasoning. In *Pro-*
596 *ceedings of the 62nd Annual Meeting of the Association for Computational Linguistics (Volume*
597 *1: Long Papers)*, pp. 12824–12840, 2024.
598
599
600
601
602
603
604
605
606
607
608
609
610
611
612
613
614
615
616
617
618
619
620
621
622
623
624
625
626
627
628
629
630
631
632
633
634
635
636
637
638
639
640
641
642
643
644
645
646
647

648 A THEORETICAL ANALYSIS

649 650 A.1 SCHEMA INDUCTION: A MECHANISTIC ANALYSIS OF STRUCTURAL PROPERTIES

651
 652 We analyze our **Schema-aware Segment Induction**, a theoretically grounded mechanism that intro-
 653 duces two inductive biases essential for table representation learning: (1) *Header–Value Coupling*,
 654 which enforces schema–value dependencies and preserves token roles, thereby realizing **Structural**
 655 **Fidelity**; and (2) *Segment-Order Equivariance*, which treats rows as sets of header–value segments
 656 and removes spurious order dependence, thereby realizing **Structural Consistency**.

657 658 STRUCTURAL FIDELITY VIA SCHEMA-CONSISTENT ATTENTION ROUTING

659 **Setup.** For segment k with header $h^{(k)}$, let the token representation be

$$660 \quad z_p = z_{\text{base}} + E_{\text{global}}(h^{(k)}),$$

661 where z_{base} contains word and positional embeddings and $E_{\text{global}}(h^{(k)})$ is the universal header
 662 embedding. Queries and keys are linear maps $Q_p = W_Q z_p$, $K_q = W_K z_q$.

663 **Analysis.** Let the token representation for p in segment k be

$$664 \quad z_p = b_p + E, \quad b_p := z_{\text{base},p}, \quad E := E_{\text{global}}(h^{(k)}).$$

665 With $Q_p = W_Q z_p$, $K_q = W_K z_q$ and $M := W_Q^\top W_K$, the attention logit expands to

$$666 \quad \begin{aligned} \ell_{pq} &= Q_p^\top K_q = (b_p + E)^\top M (b_q + E) \\ 667 &= b_p^\top M b_q + b_p^\top M E + E^\top M b_q + E^\top M E. \end{aligned} \quad (1)$$

668 The quadratic term $E^\top M E$ is independent of (p, q) and thus acts as a *shared, header-dependent*
 669 *bias* within the entire segment k . The two cross-terms vary with p, q , but under LayerNorm (Ba
 670 et al., 2016) ($\mathbb{E}[b_p] = \mathbb{E}[b_q] = 0$) their expectations vanish. Hence the expected logit decomposes as

$$671 \quad \mathbb{E}_{p,q} \ell_{pq} = \mathbb{E}_{p,q} [b_p^\top M b_q] + E^\top M E,$$

672 where the second term is the segment-wide bias.

673 Gradient w.r.t. E , Differentiating equation 1 gives

$$674 \quad \nabla_E \ell_{pq} = M b_q + M^\top b_p + (M + M^\top) E.$$

675 Averaging over all (p, q) within the segment yields

$$676 \quad \mathbb{E}_{p,q} \nabla_E \ell_{pq} = (M + M^\top) E,$$

677 since $\mathbb{E}[b_p] = \mathbb{E}[b_q] = 0$. Thus, the expected update direction is the same for all tokens in the
 678 segment, depending only on E and the projection matrices.

679 Since the MSM loss is token-level cross-entropy and analytically unwieldy, we study a surrogate
 680 quadratic objective $\mathcal{J}(E)$ that isolates the effect of header embeddings on attention logits.

$$681 \quad \mathcal{J}(E) := \sum_{p,q} \ell_{pq} = \sum_{p,q} b_p^\top M b_q + 2E^\top M \sum_q b_q + |S_k|^2 E^\top \text{Sym}(M) E,$$

682 where $|S_k|$ is the number of tokens in the segment. The stationary point satisfies

$$683 \quad \nabla_E \mathcal{J}(E) = 2M \sum_q b_q + 2|S_k|^2 \text{Sym}(M) E = 0,$$

684 so that

$$685 \quad E^* = -(|S_k|^2 \text{Sym}(M))^{-1} M \sum_q b_q.$$

686 With LayerNorm, $\sum_q b_q \approx 0$, making the optimizer align with the quadratic term $E^\top \text{Sym}(M) E$.

687 **Conclusion.** Adding $E_{\text{global}}(h^{(k)})$ to all tokens yields a shared quadratic bias $E^\top \text{Sym}(M) E$
 688 independent of values, and a uniform update direction $(M + M^\top) E$. Together, these reinforce
 689 schema–value coupling consistently across tokens in a segment, ensuring **Structural Fidelity**.

702 STRUCTURAL CONSISTENCY VIA EQUIVARIANCE
703

704 **Setup.** Each row is serialized as a set of header–value segments $\{s(r, h_k)\}$, with segment-wise
705 positional encodings but no global positions. Thus the encoder $g(\cdot)$ processes each segment inde-
706 pendently, without reference to their global order.

707 **Analysis.** Since each segment is processed locally, the encoder g is *permutation-equivariant*:

$$709 \quad g(\pi \cdot \{s(r, h_k)\}) = \pi \cdot g(\{s(r, h_k)\}).$$

711 For any permutation π , the encoder output followed by a permutation-invariant readout ρ , specifi-
712 cally mean pooling over segment embeddings, satisfies

$$714 \quad f_{\text{mean-pool}}(r) = \rho \left(\sum_k \phi(s(r, h_k)) \right),$$

717 which matches the functional form of Deep Sets (Zaheer et al., 2017), with $\phi = g$ and ρ the pooling.
718 By the universal approximation theorem for Deep Sets, f_{mean} can approximate any continuous
719 permutation-invariant function over sets of segments.

720 Let z_{cls} be the row token. One self–attention update is

$$722 \quad z'_{\text{cls}} = \sum_q \alpha_{\text{cls} \rightarrow q} V_q, \quad \alpha_{\text{cls} \rightarrow q} = \frac{\exp(\ell_{\text{cls},q}/\tau)}{\sum_{q'} \exp(\ell_{\text{cls},q'}/\tau)}, \quad \ell_{\text{cls},q} = (W_Q z_{\text{cls}})^\top (W_K z_q). \quad (2)$$

725 For any permutation π of segments in the row, the value/key sequences are merely reindexed:

$$727 \quad \{(z_q, V_q)\}_q \mapsto \{(z_{\pi(q)}, V_{\pi(q)})\}_q \quad \Rightarrow \quad \{\ell_{\text{cls},q}\}_q \mapsto \{\ell_{\text{cls},\pi(q)}\}_q \quad \Rightarrow \quad \{\alpha_{\text{cls} \rightarrow q}\}_q \mapsto \{\alpha_{\text{cls} \rightarrow \pi(q)}\}_q.$$

729 Plugging the reindexed weights/values into equation 2 gives

$$731 \quad z'_{\text{cls}}(\pi \cdot \{s(r, h_k)\}) = \sum_q \alpha_{\text{cls} \rightarrow \pi(q)} V_{\pi(q)} = \sum_q \alpha_{\text{cls} \rightarrow q} V_q = z'_{\text{cls}}(\{s(r, h_k)\}),$$

733 so the CLS update is permutation *invariant* when the operation is a pure reindexing (no extra biases,
734 identical residual paths, exact arithmetic).

735 *Relaxation to ε –stability.* In practice, residual connections, layernorm/biases and finite precision
736 introduce small deviations. We measure these by the permutation sensitivity index (PSI):

$$738 \quad \text{PSI} = \mathbb{E}_\pi [1 - \cos(f(r), f_\pi(r))],$$

739 with $f(r)$ the row embedding (CLS or mean-pooled) and $f_\pi(r)$ after permuting segments by π . We
740 say the encoder is ε –*permutation-stable* if $\text{PSI} \leq \varepsilon$.

742 **Conclusion.** Mean pooling yields $f(r) = \rho(\sum_k \phi(s(r, h_k)))$, targeting invariance. For CLS, the
743 derivation above shows invariance in the ideal limit and *strong approximate* invariance in practice,
744 with ε empirically small (Table 3). Hence both readouts achieve **Structural Consistency**.

745
746
747
748
749
750
751
752
753
754
755

756 A.2 CONTRASTIVE ALIGNMENT: GEOMETRIC FOUNDATIONS OF DOMAIN PROPERTIES
757758 We analyze Entropy-driven Segment Alignment, an InfoNCE-based objective that provably induces
759 **domain manifold** geometry in the segment embedding space. Building on the alignment–uniformity
760 framework of Wang & Isola (2020), we show:761

- 762 • Low-entropy (domain-coherent) columns are contracted toward its corresponding semantic
763 centroids, forming a cross-table domain anchors rather than table-specific clusters. This
764 realizes entropy-aware alignment and thereby **Domain Consistency**.
- 765 • High-entropy (entity-specific) columns experience entropy-aware uniformity: ESA repels
766 rows away from one another, but in a controlled manner that keeps them contained within
767 the same domain. This realizes **Domain Fidelity** by preserving row-level separability.

768 These guarantees provide the theoretical foundation for the empirical patterns in Figure 4, **low entropy** (schema-stable)
769 segments contract onto semantic centroids as anchors, forming a cross-table
770 **domain manifold**, while high-entropy (entity-specific) segments spread across this manifold in a
771 uniform manner.772 PRELIMINARIES
773774 Let $(\mathcal{T}, \mathcal{F}, P)$ be a probability space over tables, where \mathcal{T} denotes the set of admissible tables, \mathcal{F}
775 is a σ -algebra, and P is a probability measure capturing the empirical distribution of tables. An
776 encoder $f_\theta : \mathcal{T} \rightarrow \mathcal{V}$ maps each table $T \in \mathcal{T}$ into a metric space (\mathbb{R}^d, D) , where \mathcal{V} denotes the
777 representation space endowed with distance D . We adopt the following assumptions:778

- 779 (A1) **(Normalization)** All embeddings $E_{\text{seg}}(\cdot)$, $V_{\text{ctx}}(\cdot)$, and $E_{\text{global}}(\cdot)$ are ℓ_2 -normalized, i.e., lie
780 on the unit sphere $\mathbb{S}^{d-1} \subset \mathbb{R}^d$.
- 781 (A2) **(Geometry)** The distance metric is the cosine distance $D(u, v) = 1 - u^\top v$, inducing a
782 geodesic structure consistent with the sphere.
- 783 (A3) **(Information-Theoretic Objective)** The InfoNCE loss uses in-batch negative sampling suf-
784 ficiently dense over rows, approximating a variational lower bound on mutual information.
- 785 (A4) **(Optimization)** The temperature $\tau > 0$ is fixed, scaling contrastive forces smoothly.
- 786 (A5) **(Entropy Estimation)** Column entropy is estimated from the empirical distribution. Misclas-
787 sification probability decays exponentially in the number of rows (via large deviation bounds).

788 ENTROPY-AWARE ALIGNMENT AND UNIFORMITY
789790 Following Wang & Isola (2020), contrastive learning can be understood via two functionals: *alignment*,
791 the expected closeness of positive pairs, and *uniformity*, the spreading of representations
792 across the unit sphere. We adapt these notions by conditioning on column entropy.793 **Notation.** For a column c , let $\mu_c := E_{\text{global}}(h_c)/\|E_{\text{global}}(h_c)\|$ be its normalized global header
794 (**semantic** centroid). Let $\mathcal{N}_{\text{cent}}(c) = \{\mu_{c'} : c' \neq c\}$ denote centroids of other headers. For high-
795 entropy columns, let $v(r, h_c) := V_{\text{ctx}}(r, h_c)/\|V_{\text{ctx}}(r, h_c)\|$ be the normalized contextual value.796 **Definition 1** (Domain Consistency (entropy-aware alignment)). *For $c \in \mathcal{C}_{\text{low}}$, positives are centroid
797 pairs $(s(r, h_c), \mu_c)$. Define*

800
$$\mathcal{L}_{\text{align}}^{\text{low}}(f; \alpha) := \mathbb{E}_r \|s(r, h_c) - \mu_c\|_2^\alpha.$$

801

802 The model is ϵ_{con} -consistent if $\mathcal{L}_{\text{align}}^{\text{low}} \leq \epsilon_{\text{con}}$.
803804 **Definition 2** (Domain Fidelity (entropy-aware uniformity)). *For $c \in \mathcal{C}_{\text{high}}$, the positive is
805 $(s(r, h_c), v(r, h_c))$ and negatives are $(s(r, h_c), v(r', h_c))$ with $r' \neq r$. Dispersion is measured by*
806

807
$$\mathcal{L}_{\text{unif}}^{\text{high}}(f; t) := \log \mathbb{E}_{r \neq r'} \exp(-t \|s(r, h_c) - s(r', h_c)\|_2^2).$$

808

809 The model is ϵ_{dom} -faithful if $\mathcal{L}_{\text{unif}}^{\text{high}} \geq -\epsilon_{\text{dom}}$.

810 **Assumptions for Entropy Partition.** $\mathcal{C}_{\text{low}} = \{c : H(c) \leq H_0\}$ and $\mathcal{C}_{\text{high}} = \{c : H(c) \geq H_1\}$
 811 with $H_0 < H_1$. For $c \in \mathcal{C}_{\text{low}}$, positives are $(s(r, h_c), \mu_c)$ and negatives are $(s(r, h_c), \mu_c^-)$ with $\mu_c^- \in$
 812 $\mathcal{N}_{\text{cent}}(c)$. For $c \in \mathcal{C}_{\text{high}}$, positives are $(s(r, h_c), v(r, h_c))$ and negatives are $(s(r, h_c), v(r', h_c))$.
 813

814 **Assumption 1 (MI gap – centroid/value forms).** There exist $\Delta_{\text{pos}}, \Delta_{\text{neg}} > 0$ s.t.
 815

$$\begin{aligned} \mathbb{E}\langle s, \mu_c \rangle - \mathbb{E}\langle s, \mu_c^- \rangle &\geq \Delta_{\text{pos}} \quad (c \in \mathcal{C}_{\text{low}}) \\ \mathbb{E}\langle s, v(r', h_c) \rangle - \mathbb{E}\langle s, v(r, h_c) \rangle &\geq \Delta_{\text{neg}} \quad (c \in \mathcal{C}_{\text{high}}). \end{aligned}$$

819 **Assumption 2 (Entropy estimation).** $\Pr(\sup_c |\hat{H}(c) - H(c)| \leq C \sqrt{\frac{\log(1/\delta)}{m_c}}) \geq 1 - \delta$.
 820

821 **Theorem 1 (Domain Consistency–Fidelity Guarantee).** Suppose Assumptions 1–2 hold and let θ^*
 822 satisfy $\mathcal{L}_{\text{align}}(\theta^*) \leq \eta$. Then there exist functions ϕ_1, ϕ_2 with ϕ_i nondecreasing in η, τ and nonin-
 823 creasing in B such that

$$\sup_{c \in \mathcal{C}_{\text{low}}} \mathcal{L}_{\text{align}}^{\text{low}}(f; \alpha) \leq \phi_1(\eta, \tau, B) = \frac{1}{\Delta_{\text{pos}}} \psi_1(\eta, \tau, B), \quad (3)$$

$$\inf_{c \in \mathcal{C}_{\text{high}}} \mathcal{L}_{\text{unif}}^{\text{high}}(f; t) \geq \phi_2(\eta, \tau, B) = \frac{1}{\Delta_{\text{neg}}} \psi_2(\eta, \tau, B), \quad (4)$$

824 where $\psi_i(\eta, \tau, B) = (\tau(\eta - \log B))_+$. Moreover, with prob. $\geq 1 - \delta$, any $\hat{\theta}$ with $\hat{\mathcal{L}}_{\text{align}}(\hat{\theta}) \leq \hat{\eta}$ and
 825 $\|\nabla \hat{\mathcal{L}}_{\text{align}}(\hat{\theta})\| \leq \varepsilon$ satisfies the same bounds with $\eta = \hat{\eta} + \mathfrak{R}_n + O(\varepsilon)$, $\mathfrak{R}_n = O(\sqrt{\log(1/\delta)/n})$.
 826

827 *Proof.* On \mathbb{S}^{d-1} , $D(u, v) = 1 - \langle u, v \rangle$. The population InfoNCE risk for batch B , temperature τ is
 828

$$\mathcal{L}_{\text{align}}(\theta) = \mathbb{E} \left[-\log \frac{e^{\langle s, s^+ \rangle / \tau}}{e^{\langle s, s^+ \rangle / \tau} + \sum_{j=1}^{B-1} e^{\langle s, s_j^- \rangle / \tau}} \right]. \quad (5)$$

829 For any $a, b_1, \dots, b_m \in \mathbb{R}$ and $\tau > 0$, the Softmax–margin inequality (Saunshi et al., 2019) is
 830

$$-\log \frac{e^{a/\tau}}{e^{a/\tau} + \sum_{j=1}^m e^{b_j/\tau}} \leq \frac{1}{\tau} \max_j (b_j - a) + \log(1 + m). \quad (6)$$

831 **(Alignment, contraction of low entropy segments).** Apply equation 6 to equation 5 with $a = \langle s, \mu_c \rangle$,
 832 $b_j = \langle s, \mu_c^{-(j)} \rangle$ to obtain $\mathbb{E}\langle s, \mu_c \rangle - \mathbb{E}\langle s, \mu_c^- \rangle \geq \tau(\log B - \eta)$. By Assumption 1 and $\|u - \mu\|_2^2 =$
 833 $2(1 - \langle u, \mu \rangle)$,

$$\mathbb{E}_r \|s(r, h_c) - \mu_c\|_2^2 \leq \frac{2}{\Delta_{\text{pos}}} \psi_1(\eta, \tau, B). \quad (7)$$

834 **(Uniformity, repulsion of high entropy segments).** Set $a = \langle s, v(r, h_c) \rangle$, $b_j = \langle s, v(r_j, h_c) \rangle$; then
 835 $\mathbb{E}\langle s, v(r', h_c) \rangle - \mathbb{E}\langle s, v(r, h_c) \rangle \geq \tau(\log B - \eta)$. Assumption 1 yields
 836

$$\log \mathbb{E}_{r \neq r'} \exp(-t \|s(r, h_c) - s(r', h_c)\|_2^2) \geq \frac{1}{\Delta_{\text{neg}}} \psi_2(\eta, \tau, B). \quad (8)$$

837 For finite-sample, uniform convergence (Saunshi et al., 2019) gives
 838

$$\sup_{\theta} \left| \hat{\mathcal{L}}_{\text{align}}(\theta) - \mathcal{L}_{\text{align}}(\theta) \right| \leq \mathfrak{R}_n = O\left(\sqrt{\frac{\log(1/\delta)}{n}}\right) \text{ w.p. } \geq 1 - \delta. \quad (9)$$

839 If $\hat{\mathcal{L}}_{\text{align}}(\hat{\theta}) \leq \hat{\eta}$ and $\|\nabla \hat{\mathcal{L}}_{\text{align}}(\hat{\theta})\| \leq \varepsilon$, smoothness implies
 840

$$\mathcal{L}_{\text{align}}(\hat{\theta}) \leq \hat{\eta} + \mathfrak{R}_n + O(\varepsilon). \quad (10)$$

841 Set $\tilde{\eta} := \hat{\eta} + \mathfrak{R}_n + O(\varepsilon)$ and substitute $\eta = \tilde{\eta}$ into equation 7 and equation 8. Routing by $\hat{H}(c)$
 842 and Assumption 2 give a misrouting probability δ_{ent} that vanishes with m_c , so the bounds hold with
 843 prob. $\geq 1 - \delta - \delta_{\text{ent}}$. \square

864 **Corollary 1** (Entropy-aware Alignment \Rightarrow Domain Consistency). *With probability at least $1 - \delta - \delta_{\text{ent}}$, if η is small and B is large, then*

865
$$\mathcal{L}_{\text{align}}^{\text{low}}(f; \alpha) \leq \tilde{O}\left(\frac{\tau}{\Delta_{\text{pos}} B}\right),$$

866 *so low-entropy columns contract toward their semantic centroids, ensuring **Domain Consistency**.*

867 **Corollary 2** (Entropy-aware Uniformity \Rightarrow Domain Fidelity). *Under the same conditions,*

868
$$\mathcal{L}_{\text{unif}}^{\text{high}}(f; t) \geq \tilde{\Omega}\left(\frac{1}{\tau} \Delta_{\text{neg}}\right),$$

869 *so high-entropy columns preserve row-level separation, ensuring **Domain Fidelity**.*

870 *Remark.* Taken together, these corollaries formalize the *domain manifold geometry* induced by entropy-driven segment alignment: **low-entropy** (schema-stable) segments contract onto a shared **cross-table manifold**, while **high-entropy** (entity-specific) segments distribute across this manifold with entropy-aware uniformity. This structure preserves domain-level coherence while maintaining row-level discriminativity. Here $\tilde{O}(\cdot)$ and $\tilde{\Omega}(\cdot)$ suppress polylogarithmic factors in n .

871
872
873
874
875
876
877
878
879
880
881
882
883
884
885
886
887
888
889
890
891
892
893
894
895
896
897
898
899
900
901
902
903
904
905
906
907
908
909
910
911
912
913
914
915
916
917

918 **B RELATED WORKS**
919920 **B.1 FIDELITY-ORIENTED ENCODERS**
921922 A significant body of research has focused on developing structure-aware encoders, which attempt
923 to explicitly model the 2D layout and relational structure of tables. While foundational, these ap-
924 proaches commonly suffer from two major drawbacks; Inefficiency and Inconsistency.925 Inefficiency arises from the architectural complexity required to capture structural cues. These
926 models often introduce significant computational and training overhead. TAPAS Herzig et al.
927 (2020), for example, employs a multitude of embedding layers to encode token roles (e.g., `row_id`,
928 `column_id`, `rank_id`), which is expensive to train. TaBERT Yin et al. (2020) linearizes table
929 content, but its representation is suboptimal; embedding a single cell $\langle i, j \rangle$ requires a minimum
930 of three tokens. For real-world tables with hundreds of columns, this approach quickly becomes
931 infeasible within standard token limits. Other models introduce complexity through architectural
932 choices, such as Tabbie Iida et al. (2021) utilizing two separate transformers, or through intricate
933 encoding schemes. Turl Deng et al. (2022) uses a complex entity representation process involving
934 two role embeddings (type and mention) and a projection layer. Tuta Wang et al. (2021) imple-
935 ments a highly complex positional encoding system with multiple levels of independently learned,
936 tree-based positional encodings, in addition to in-cell positional encodings.
937

Despite this added complexity, these models fail to achieve robust semantic consistency. Their representations remain vulnerable to simple schema variations, such as column reordering. Furthermore, the embeddings for a given concept can drift semantically depending on the specific query or the context of neighboring entities, indicating a lack of true semantic grounding.

941 **B.2 CONSISTENCY-ORIENTED ENCODER**
942943 More recently, research has shifted toward domain-aware encoders, which prioritize semantic con-
944 sistency across different table structures, aiming to capture the “domain” of a column. A notable
945 example is HAETAE Jung & Yoon (2025), which contrasts with structure-aware models by using
946 a simpler, lightweight approach. It uses a standard BERT backbone but integrates an additional
947 embedding layer for row context-free header tokens. Haetae trains this universal header embedding
948 using a distance-based objective, which explicitly forces headers with the same semantic meaning
949 (e.g., “First Name” and “f_name”) to have similar representations.950 While this method successfully ensures header consistency, it introduces a critical limitation:
951 Header-value Misalignment. By forcing header representations to be close while neglecting the
952 semantic information contained in the cell values, the model harms the crucial header-value depen-
953 dencies. This optimization for header-level consistency weakens the model’s ability to perform deep
954 table reasoning. The resulting consistency is not truly grounded in the full domain semantics of the
955 table, as it largely ignores the values, which are essential for defining that domain.956 **B.3 TASK-ORIENTED APPROACHES**
957958 A line of research focuses on task-specific pretraining, adapting language models to address the
959 heterogeneity of tabular attributes for supervised prediction. TP-BERTa (Yan et al.), for example, is
960 designed explicitly for regression and classification, introducing relative magnitude tokenization and
961 intra-feature attention to reconcile numerical values with feature semantics, thereby competing with
962 strong tree-based and deep tabular baselines. Complementary paradigms expand task awareness in
963 different directions: TAPEX (Liu et al.) pretrains on SQL execution to enhance table QA, while
964 TabPFN (Hollmann et al.) uses synthetic priors for probabilistic classification without finetuning.
965 More recent work pushes toward broader reasoning capabilities, including modular table reason-
966 ing with TAPERa (Zhao et al., 2024), instruction-tuned multi-task alignment in Table-GPT (Li
967 et al., 2024), and generative modeling with CDTD (Mueller et al., 2023) for mixed-type imputa-
968 tion. Collectively, these efforts highlight a shift toward tailoring pretraining to specific downstream
969 tasks—whether predictive modeling, QA, or imputation—though such specialization often comes at
970 the cost of limited transferability across domains requiring general-purpose table understanding.

971

972 **C SUPPLEMENTARY ANALYSES**
973974 **C.1 FIDELITY UNDER SCHEMA PERTURBATIONS**
975976 To complement the fidelity analysis in Section 3.2, we further evaluate NAVI’s robustness under
977 schema perturbations that mimic realistic inconsistencies in web tables. While the main paper
978 evaluates fidelity on clean schemas, practical deployments must handle lexical drift (e.g., syn-
979onyms), noisy or unseen headers (e.g., typos), and structural variation (e.g., column reordering). We
980 therefore apply controlled perturbations at inference time—using models trained strictly on clean
981 schemas—to test whether NAVI preserves both domain fidelity (entity-level discriminability) and
982 structural fidelity (schema–value grounding) under degraded schema conditions.983 We consider three perturbation types commonly observed in heterogeneous table corpora:
984985

- 986 **Synonym replacement (semantic OOV).** For each table, we identify low-entropy headers
987 and randomly replace 50% of them with semantically equivalent yet unseen alternatives
988 from a curated synonym mapping (e.g., director.name → auteur.name). This tests whether
989 semantic variants map to the same header manifold region.
- 990 **Header typos (noisy OOV).** We sample 50% of low-entropy headers and apply 1–2
991 character-level corruptions (substitution, insertion, deletion), producing unseen, noisy
992 forms that break lexical structure. This simulates genuinely OOV headers rather than sim-
993 ple lexical variants.
- 994 **Column reordering (structural noise).** For each row, we randomly permute the column
995 order while preserving header–value associations. This tests whether NAVI’s row repre-
996 sentations are sensitive to presentation order.

997
998 **Table 5: F1 Score on Row Classification with XGBoost (domain fidelity) and Accuracy on Value**
999 **Imputation (structural fidelity) for both Product and Movie domains).**
10001001
1002
1003
1004
1005
1006
1007
1008
1009

Model	Product		Movie	
	R-Cls (F1)	Val (acc.)	R-Cls (F1)	Val (acc.)
Default	0.9301	0.7902	0.6394	0.7077
Synonym	0.9466	0.7743	0.6322	0.6918
Typo	0.9284	0.7212	0.6103	0.6620
Column Reordered	0.9404	0.7830	0.6161	0.7007

1010 Synonym replacement yields performance essentially matching or slightly exceeding the clean-
1011 schema baseline (e.g., Product Cls: 0.9295 → 0.9466), indicating that NAVI’s global header en-
1012 coder effectively absorbs semantic variants and maps them to the same low-entropy centroids. This
1013 aligns with our consistency analysis: synonym-level drift has minimal effect on the semantic man-
1014 ifold structure. Header typos produce the largest degradation (e.g., Movie Cls: 0.6394 → 0.6103),
1015 as expected when character corruption disrupts subword tokenization and weakens header–value
1016 grounding. Nonetheless, NAVI retains a substantial portion of its clean-schema fidelity—far from
1017 catastrophic failure—demonstrating that entropy-aware alignment provides robust anchoring even
1018 under noisy OOV headers. Column reordering results in only minor changes, with performance
1019 consistently close to the clean baseline (e.g., Prod Imp: 0.7857 → 0.7830). This confirms NAVI’s
1020 row-as-multiset design: segment-based representations are largely insensitive to column order, pre-
1021 serving both domain and structural fidelity under presentation-level variability.1022 Overall, these results show that NAVI’s fidelity is highly stable under realistic schema inconsis-
1023 tencies. Semantic variations (synonyms) are effectively normalized; structural perturbations (reorder-
1024 ing) have negligible impact; and even noisy OOV cases (typos) degrade performance gracefully
1025 rather than collapsing schema–value grounding. These findings reinforce that entropy-aware align-
1026 ment yields a durable, schema-robust representation of table semantics.

1026
1027

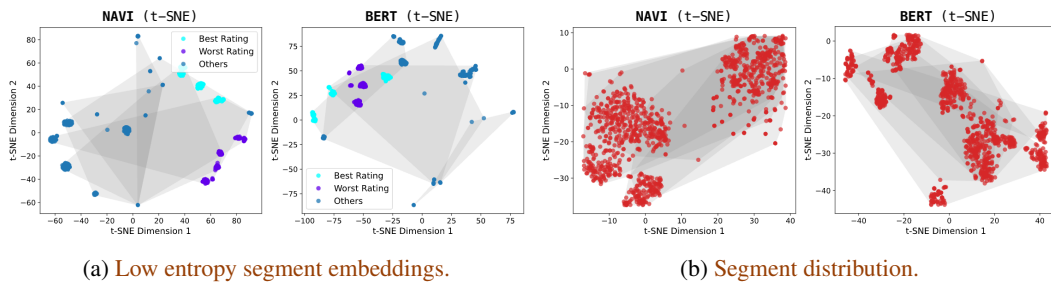
C.2 GEOMETRY OF SEGMENT EMBEDDINGS

1028
1029
1030
1031
1032
1033

To further examine how NAVI organizes segment-level representations, we visualize segments from five Movie tables using t-SNE, grouping segments by their entropy category (low vs. high) and overlaying table-wise convex hulls (Figure 5). The resulting geometry provides qualitative evidence that NAVI realizes cross-table generalization (*domain consistency, domain fidelity*). For BERT, segment embeddings are constructed by mean-pooling the contextualized token embeddings of each header–value span, ensuring a comparable segment representation across models.

1034
1035
1036
1037

Figure 5: t-SNE projections of header–value segment embeddings from five Movie tables, grouped by entropy category. Gray convex hulls correspond to individual tables. For low entropy segments, points are additionally labeled as Best Rating or Worst Rating.

1038
1039
1040
1041
1042
1043
10441045
1046

Low-entropy segments correspond to stable domain concepts (e.g., ratings, director). To assess whether models recover these semantics, we color segments using two coherent groups—Best Rating and Worst Rating. Under NAVI, the two groups form clean, well-separated clusters that persist across tables, with overlapping convex hulls indicating that the geometry is driven by shared cross-table value distributions rather than table identity. This reflects strong semantic discrimination and domain-level invariance. Quantitatively, NAVI attains a higher silhouette score (0.7061) than BERT (0.2327), confirming that BERT’s clusters remain overlapping and weakly delineated, dominated by table-specific structure. Overall, NAVI collapses surface-form variation while preserving core domain distinctions, yielding representations that generalize consistently across heterogeneous tables.

1047
1048
1049
1050
1051
1052
1053
1054
1055
1056
1057
1058
1059
1060
1061
1062

High-entropy segments represent entity-specific content (e.g., names, descriptions). NAVI distributes these segments broadly, avoiding collapse even when within-table contexts are similar. The table hulls heavily overlap, showing that representations do not cling to table identity. BERT, however, forms several dense, table-specific clumps, indicating that its contextual embedding remains sensitive to table-local patterns and fails to maintain row-level separability across tables. NAVI’s geometry thus reflects stronger domain fidelity: entity-specific values remain distinguishable without being entangled with schema or table-specific quirks.

1063

D IMPLEMENTATION DETAILS

1064

D.1 ARCHITECTURAL DETAILS

1065

Global Header Encoder The header encoder is implemented as a lightweight BERT-based module that generates context-independent embeddings for header strings. The encoder utilizes BERT tokenizer and embedding layer, followed by two transformer layers (layers 8 and 9 from the pre-trained BERT model) to capture semantic representations of header names, **effectively leveraging BERT’s semantic priors**.

1073
1074
1075
1076

The design choice of using two layers strikes a balance between expressivity and efficiency: a shallow encoder reduces computational overhead while still allowing non-trivial contextualization beyond the embedding layer. Using more layers risks overfitting to sentence-level semantics irrelevant for headers, while fewer layers (e.g., only one) limit the ability to model compositional structure.

1077
1078
1079

The selection of layers 8 and 9 is grounded in empirical analysis of BERT (Clark et al., 2019) shows that mid-to-deep layers (approximately layers 7–10) specialize in syntactic dependencies and head–dependent relations, such as determiners linking to nouns and direct objects linking to verbs. By contrast, earlier layers capture mostly local or lexical information, while the final layers (11–12)

1080 are biased toward [CLS]-based sentence aggregation and task-specific adaptation. Leveraging layers
 1081 8 and 9 thus provides a strong inductive bias for modeling headers, which are typically short noun
 1082 phrases requiring syntactic but not full discourse-level context.

1083 Given a header string h , the encoder first tokenizes it using the BERT tokenizer, then processes the
 1084 tokens through the embedding layer to obtain initial representations. These embeddings are passed
 1085 through two sequential transformer layers with self-attention mechanisms:

$$\begin{aligned} \mathbf{h}^{(0)} &= \text{BertEmbeddings}(\text{tokenize}(h)) \\ \mathbf{h}^{(1)} &= \text{EncoderLayer}_8(\mathbf{h}^{(0)}) \\ \mathbf{h}^{(2)} &= \text{EncoderLayer}_9(\mathbf{h}^{(1)}) \end{aligned}$$

1090 The final universal header embedding $E_{\text{global}}(h)$ is obtained through mean pooling over the sequence
 1091 dimension, weighted by the attention mask to exclude padding tokens:

$$E_{\text{global}}(h) = \frac{\sum_{i=1}^n \mathbf{h}_i^{(2)} \cdot \text{mask}_i}{\sum_{i=1}^n \text{mask}_i}.$$

1095 The encoder supports flexible input formats, handling single header strings, flat lists of headers, or
 1096 batched lists, automatically adjusting the output dimensionality and providing appropriate masking
 1097 for batch processing.

1099 **Projection Layer for Segments** The segment projection network $g(\cdot)$ implements the transformation
 1100 that combines universal header embeddings, contextualized header representations, and contextu-
 1101 alized value representations into unified segment embeddings. Motivated by projection layers
 1102 in transformer-based language models (Vaswani et al., 2017), the architecture adopts a two-stage
 1103 feedforward block with residual connections and normalization, enabling non-linear feature mixing
 1104 while maintaining training stability.

1105 Given the three input components $E_{\text{global}} \in \mathbb{R}^{B \times H \times D}$, $H_{\text{ctx}} \in \mathbb{R}^{B \times H \times D}$, and $V_{\text{ctx}} \in \mathbb{R}^{B \times H \times D}$, the
 1106 projection first concatenates them along the feature dimension:

$$\mathbf{x}_{\text{concat}} = [E_{\text{global}} \parallel H_{\text{ctx}} \parallel V_{\text{ctx}}] \in \mathbb{R}^{B \times H \times 3D}$$

1109 The concatenated representation is then processed through a two-layer feedforward network with
 1110 GELU activation and layer normalization:

$$\begin{aligned} \mathbf{x}_{\text{hidden}} &= \text{LayerNorm}(\text{GELU}(\text{Linear3D} \rightarrow 2D(\mathbf{x}_{\text{concat}}))) \\ s(r, h) &= \text{LayerNorm}(\text{Linear2D} \rightarrow D(\text{Dropout}(\mathbf{x}_{\text{hidden}}))) \end{aligned}$$

1113 This design mirrors the intermediate expansion–compression scheme used in transformers, where
 1114 increasing dimensionality allows richer interactions between features before reducing back to the
 1115 model dimension for compatibility. By concatenating schema-level and row-level signals, the pro-
 1116 jection network learns to fuse global header semantics with local contextual patterns. The residual
 1117 normalization ensures stable optimization, while the intermediate $2D$ bottleneck provides sufficient
 1118 capacity to capture complex header–value dependencies.

1120 D.2 DATASET PREPROCESSING

1121 Our dataset preprocessing pipeline is designed to optimize the quality and compatibility of tabular
 1122 data for BERT-based language model training. The preprocessing consists of three main stages: data
 1123 cleaning, BERT vocabulary validation, and tokenization optimization.

1125 **Data Cleaning and Normalization** The raw tabular data undergoes several cleaning steps to en-
 1126 sure consistency and quality. First, we flatten nested JSON structures. For example:

```
1127 "actors": [ { "name": "allan" }, { "name": "daniel" } ] →
1128   "actors.0.name": "allan", "actors.1.name": "daniel"
```

1130 This creates a uniform representation where each row is represented as a flat dictionary of key-value
 1131 pairs. This flattening process preserves the hierarchical structure through dot-separated keys.

1132 Next, we handle indexed fields that represent repeated attributes. To prevent information overload
 1133 and maintain computational efficiency, we sample a maximum of 3 indexed fields per field type,
 prioritizing the first occurrences to maintain data consistency.

1134 **BERT Vocabulary Validation** A critical challenge in training BERT on multilingual tabular data
 1135 is the model’s limited vocabulary coverage for non-English languages. To address this, we imple-
 1136 ment a BERT vocabulary validation step that filters out tables containing content that cannot be
 1137 effectively tokenized by the BERT tokenizer.

1138 For each table, we extract meaningful text fields (excluding URLs, pure numbers, and very short
 1139 strings) and tokenize them using the BERT tokenizer. We calculate the ratio of unknown tokens
 1140 ([UNK]) to total tokens for each field. Tables where more than 30% of the text fields contain exces-
 1141 sive unknown tokens (threshold: 30% UNK ratio) are excluded from training. This filtering ensures
 1142 that the model trains on data it can meaningfully process, significantly reducing the proportion of
 1143 uninformative [UNK] tokens during training.

1144
 1145 **Tokenization Optimization** Finally, to maximize the utility of the remaining data while respecting
 1146 BERT’s token limit constraints, we implement field-level truncation: Individual fields that exceed
 1147 20 tokens are truncated to fit within this limit, preserving the most important information while
 1148 maintaining field names and separators.

1149
 1150 **Preprocessing Statistics** Our preprocessing pipeline processes data from 100 different e-
 1151 commerce websites across multiple languages and domains. The BERT vocabulary validation step
 1152 typically filters out 60-70% of rows containing significant non-English content, resulting in a dataset
 1153 focused on English-language e-commerce data that can be effectively processed by BERT.

1154 The final preprocessed dataset maintains the structural information of the original tables while en-
 1155 suring compatibility with BERT’s tokenization scheme, enabling effective representation learning
 1156 for tabular data through masked language modeling objectives.

1157 This approach addresses the fundamental challenge of applying English-centric language models to
 1158 multilingual structured data, ensuring that the training process focuses on content that the model can
 1159 meaningfully learn from while preserving the rich structural information inherent in tabular data.

1160
 1161 D.3 TRAINING PROCEDURE
 1162

1163 **Batch Construction.** For each domain, we organize the 100 tables into stratified batches using
 1164 a hierarchical grouping strategy. Specifically, tables are grouped into sets of four (25 groups per
 1165 domain), with all rows in a group merged into a unified dataset. An epoch processes all groups
 1166 sequentially, with group order shuffled each time while preserving the 4-table grouping for compu-
 1167 tational efficiency. Within each group, stratified sampling assigns batch slots in proportion to table
 1168 size: $\text{batch_count}_{t_i} = \max(1, \text{round}(n_i/N \times \text{batch_size}))$, for table t_i with n_i rows out of N . This
 1169 procedure balances representation across tables, prevents larger tables from dominating training, and
 1170 ensures that even small tables contribute consistently to every batch.

1171
 1172 **Entropy-based Column Categorization** Following the entropy-based categorization described in
 1173 Section 2.3, we compute normalized Shannon entropy for each field f in table t :

$$H_{\text{norm}}(f) = \frac{-\sum_{v \in V_f} p(v) \log_2 p(v)}{\log_2 |V_f|}$$

1174 where V_f is the set of unique values for field f , and $p(v)$ is the probability of value v . The catego-
 1175 rization uses quartile-based thresholds computed per table:

1176
 1177 • Domain-coherent columns \mathcal{H}_{dom} : $H_{\text{norm}}(f) \leq Q_1$,
 1178 • Entity-discriminative columns \mathcal{H}_{ent} : $H_{\text{norm}}(f) \geq Q_3$,

1179
 1180 where domain-coherent columns represent stable, low-entropy fields capturing global domain se-
 1181 mantics (e.g., genre), entity-discriminative columns represent high-entropy fields that vary across
 1182 rows, capturing instance-specific attributes (e.g., title). This per-table categorization ensures robust
 1183 field classification regardless of table size or domain characteristics, with minimum guarantees of
 1184 at least one field per category when possible. The categorization is computed once per combined
 1185 dataset and used throughout the training of that group.

1188 **Algorithm 1** NAVI Training Procedure

1189 **Require:** Domain \mathcal{D} with tables $\{t_i\}_{i=1}^{100}$, model \mathcal{M}_θ , alignment weight λ_{align} ,
 1190 masking configuration MaskCfg

1191 **Ensure:** Trained parameters θ^*

1192 1: Initialize θ , optimizer, gradient scaler

1193 2: **for** epoch $t = 1, \dots, T$ **do**

1194 3: Partition 100 tables into groups $\mathcal{G} = \{G_1, \dots, G_{25}\}$, $|G_i| = 4$

1195 4: Shuffle group order

1196 5: **for** each group $G \in \mathcal{G}$ **do**

1197 6: **for** each table $t_i \in \mathcal{G}$ **do**

1198 7: Compute normalized entropy per field: $H_{\text{norm}}(f) = -\sum_{v \in V_f} p(v) \log p(v) / \log |V_f|$

1199 8: Categorize fields: $\mathcal{H}_{\text{dom}} = \{f : H_{\text{norm}}(f) \leq Q_1\}$, $\mathcal{H}_{\text{ent}} = \{f : H_{\text{norm}}(f) \geq Q_3\}$

1200 9: Initialize stratified sampler, Sampler(\mathcal{R}_G)

1201 10: **end for**

1202 11: **for** each batch $\mathcal{B} \sim \text{Sampler}(\mathcal{R}_G)$ **do**

1203 12: Apply masking Mask(\cdot ; MaskCfg): $\tilde{\mathbf{x}}_b, \mathbf{y}_b = \text{mask}(\mathbf{x}_b; \text{MaskCfg})$

1204 13: Forward (masked): logits, $\mathbf{L}_b = \mathcal{M}_\theta(\tilde{\mathbf{x}}_b)$

1205 14: Forward (unmasked): embeddings, $\mathbf{E}_b = \mathcal{M}_\theta(\mathbf{x}_b)$

1206 15: Extract components: $\{E_{\text{global}}, H_{\text{ctx}}, V_{\text{ctx}}\} = \text{extract}(\mathbf{E}_b)$

1207 16: Segment fusion: $s(r, h) = g(E_{\text{global}}(h) \parallel H_{\text{ctx}}(r, h) \parallel V_{\text{ctx}}(r, h))$

1208 17: Compute losses: $\mathcal{L}_{\text{msm}}^{(b)}, \mathcal{L}_{\text{dom}}^t, \mathcal{L}_{\text{ent}}^t$

1209 18: Total loss: $\mathcal{L}_{\text{total}}^{(b)} = \mathcal{L}_{\text{msm}}^{(b)} + \lambda_{\text{align}} \cdot \frac{1}{|\mathcal{B}|} \sum_{t \in \mathcal{B}} (\mathcal{L}_{\text{dom}}^t + \mathcal{L}_{\text{ent}}^t)$

1210 19: Update: $\theta \leftarrow \text{step}(\theta, \mathcal{L}_{\text{total}}^{(b)})$

1211 20: **end for**

1212 21: **end for**

1213 22: **end for**

1214 23: **return** \mathcal{M}_{θ^*}

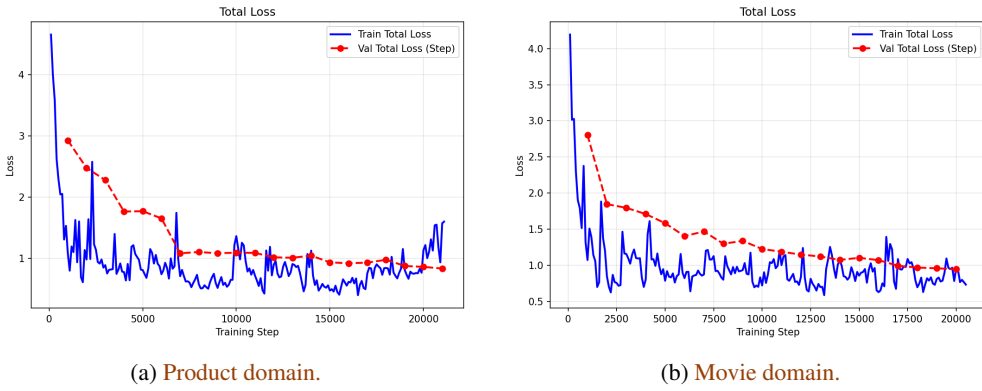
1215

1216

1217 **Masking Configuration.** Building on the structure-aware MSM framework in Section 2.2, we
 1218 define three masking regimes with token budget control: (1) Header–Value (HV) Masking: Selects
 1219 k header and value segments under a total budget $\frac{\text{max_tokens}}{\text{token_length_threshold}}$, split by a configurable
 1220 ratio (default: 50% values, 50% headers), with each segment contributing up to 8 tokens to \mathcal{M}_h
 1221 or \mathcal{M}_v . (2) BERT-style (B) Masking: Standard MLM regime with 15% uniform masking over
 1222 non-special tokens to form \mathcal{M}_r . (3) Hybrid (HVB) Masking: Combines the two by allocating
 1223 $w_{hv} \times \text{max_tokens}$ (default $w_{hv} = 0.5$) to HV masking and the remainder to BERT-style masking.
 1224 All regimes follow the usual replacement scheme (80% [MASK], 10% random, 10% unchanged).

1225 **Forward Pass and Loss Computation.** The forward pass follows the semantic-aware schema
 1226 induction framework (Section ??) and enriched by universal header embeddings described in
 1227 Appendix D.1. For each batch, the model performs two passes: (1) Masked input \rightarrow MSM logits for
 1228 structure-aware segment modeling; (2) Unmasked input \rightarrow contextualized embeddings for entropy-
 1229 aware contrastive alignment. From the unmasked pass, we extract universal header embeddings
 1230 $E_{\text{global}}(h)$, contextualized header representations $H_{\text{ctx}}(r, h)$, and value representations $V_{\text{ctx}}(r, h)$,
 1231 which are fused via the projection network $g(\cdot)$ into segment embeddings $s(r, h)$. The total loss com-
 1232 bines structure-aware MSM and entropy-aware contrastive alignment: $\mathcal{L}_{\text{total}} = \mathcal{L}_{\text{msm}} + \lambda_{\text{align}} \cdot \mathcal{L}_{\text{align}}$,
 1233 where \mathcal{L}_{msm} is computed over the masked sets \mathcal{M} , and $\mathcal{L}_{\text{align}} = \mathcal{L}_{\text{dom}}^t + \mathcal{L}_{\text{ent}}^t$ jointly enforces domain
 1234 consistency (cross-header alignment) and domain fidelity (cross-row alignment).

1235
 1236
 1237
 1238
 1239
 1240
 1241

1242 D.4 TRAINING REGIMEN AND HYPERPARAMETERS
12431244 Figure 6: Learning curves: Batch size 32 for 2 epochs, total number of steps is 21132.
12451258 Table 6: Performance of hyperparameter-tuned variants on downstream fidelity tasks. Evaluation
1259 includes Value Imputation (Val; accuracy), Row Classification with XGBoost (XGB; F1-Macro)
1260 and Logistic Regression (LR; F1-Macro). Best results per task are in bold.
1261

	Product			Movie		
	Val	XGB	LR	Val	XGB	LR
Default	0.7902	0.9295	0.9410	0.7077	0.6394	0.6667
λ_{align}						
0.01	0.7773	0.9115	0.9298	0.7009	0.5994	0.6495
0.25	0.7795	0.7513	0.8648	0.7023	0.5151	0.5615
1.25	0.7846	0.7888	0.9057	0.7046	0.3970	0.4624
$h:v:b$						
6:2:2	0.7782	0.9246	0.9359	0.7028	0.5757	0.6053
2:6:2	0.7762	0.9087	0.9379	0.7240	0.5939	0.6312
3:1:6	0.7793	0.8971	0.9289	0.7055	0.5798	0.6308
2:2:6	0.7779	0.9227	0.9399	0.7036	0.5985	0.6394
1:3:6	0.7819	0.9246	0.9388	0.6970	0.6034	0.6439
entropy thres.						
Q1/Q3	0.7789	0.9188	0.9330	0.7053	0.5043	0.5446
40p/60p	0.7204	0.8056	0.8955	0.6710	0.2236	0.3433
50p	0.7086	0.7805	0.8688	0.6460	0.1852	0.2484
$\tau_{\text{dom}}/\tau_{\text{ent}}$						
0.02/0.02	0.7716	0.9310	0.9399	0.7052	0.6174	0.6442
0.14/0.14	0.7813	0.7446	0.8829	0.7021	0.3917	0.4963
negative size						
16	0.7750	0.9228	0.9400	0.6888	0.5992	0.6396
32	0.7565	0.8959	0.9269	0.7069	0.5902	0.6078